



ORIGINAL RESEARCH

A human-robot collaboration method for uncertain surface scanning

Guanyi Zhao¹ | Chao Zeng² | Weiyong Si³ | Chenguang Yang³

¹School of Automation Science and Engineering, South China University of Technology, Guangdong, China

²TAMS Group, Department of Informatics, Universität Hamburg, Hamburg, Germany

³Bristol Robotics Laboratory, University of the West of England, Bristol, UK

Correspondence

Chenguang Yang
Email: cyang@ieee.org

Funding information

Engineering and Physical Sciences Research Council (EPSRC), Grant/Award Number: EP/S001913

Abstract

Robots are increasingly expected to replace humans in many repetitive and high-precision tasks, of which surface scanning is a typical example. However, it is usually difficult for a robot to independently deal with a surface scanning task with uncertainties in, for example the irregular surface shapes and surface properties. Moreover, it usually requires surface modelling with additional sensors, which might be time-consuming and costly. A human-robot collaboration-based approach that allows a human user and a robot to assist each other in scanning uncertain surfaces with uniform properties, such as scanning human skin in ultrasound examination is proposed. In this approach, teleoperation is used to obtain the operator's intent while allowing the operator to operate remotely. After external force perception and friction estimation, the orientation of the robot end-effector can be autonomously adjusted to keep as perpendicular to the surface as possible. Force control enables the robotic manipulator to maintain a constant contact force with the surface. And hybrid force/motion control ensures that force, position, and pose can be regulated without interfering with each other while reducing the operator's workload. The proposed method is validated using the Elite robot to perform a mock B-ultrasound scanning experiment.

KEYWORDS

medical applications, robotics

1 | INTRODUCTION

Robots are expected to perform more complex tasks in unstructured environments. However, fully autonomous robot manipulation is unlikely to be widely deployed in the foreseeable future due to current hardware and software limitations and high costs. Alternatively, human-robot collaboration (HRC) offers a more flexible, efficient, and safer solution that combines human and robot efforts to enhance robot intelligence [1–3]. More specifically, human operators and robots work together with complementary skills. Typically, robots can perform the high-precision, repetitive and dangerous tasks because they are equipped with advanced sensors and powerful computing capabilities, and humans play the role of decision-makers because they have excellent cognitive skills, extensive

experience and expertise, and can provide the robot with action guidance and error correction [4–6]. HRC has been widely used in medical care, industrial processing, search and rescue [7–9]. It has been shown that effective HRC can reduce operator workload without the need for tiring manual labour, thus improving work efficiency and quality [10, 11].

Many HRC systems have been developed recently in the robotics community. Designing an HRC system requires consideration of some key elements including interaction interfaces (e.g. teleoperation, mixed reality, and force feedback etc.) [12, 13], robot control modalities (e.g. impedance control and admittance control), system stability and security [14–16]. For instance, ref. [17] applied Electromyographic (EMG)-based HRC tasks as goal-orientation tasks to address the problem of varying muscle coordination. A novel HRC

This is an open access article under the terms of the [Creative Commons Attribution](https://creativecommons.org/licenses/by/4.0/) License, which permits use, distribution and reproduction in any medium, provided the original work is properly cited.

© 2023 The Authors. *CAAI Transactions on Intelligence Technology* published by John Wiley & Sons Ltd on behalf of The Institution of Engineering and Technology and Chongqing University of Technology.

approach with a multi-modal interface was given in ref. [18] to implement a sawing task. Zeng et al. [19] developed a bio-inspired mechanism to learn compliant robotic behaviours. The authors in refs. [20, 21] designed shared control schemes for a mobile robot with teleoperation. Rozo et al. [22] taught the robot cooperative behaviours for motion adaptation from the demonstration. Duchaine et al. [23] developed a novel variable admittance control algorithm to improve robot motion stability and intuitive human interaction.

Many contact task scenarios require surface scanning manipulation. For example, as shown in Figure 1, the ultrasonic examination is a typical surface scanning task. The main technologies involved in surface scanning include position, pose and force control. For position and pose control, three popular methods are currently used: (1) teleoperation, (2) vision-based surface modelling, and (3) demonstration-based trajectory planning [24]. The first method is very popular for involving human operation in the human-in-the-loop system while keeping them out of the working environment and improving working efficiency [25, 26]. With the progress of hardware, different kinds of teleoperation systems have been applied to HRC tasks. For instance, the operator piloted an aerial robot by augmented reality in ref. [27]. In ref. [28], the operator sent commands to robots using brain-computer interface, and the authors in ref. [29] teleoperated industrial robot to implement car body surface treatment operation with a haptic feedback device. However, if precision is required, pure teleoperation methods would be very challenging for operators. The second method generally offers higher accuracy. However, it usually relies on external vision sensors (e.g. depth cameras and stereo cameras) to collect surface data such as 3D point clouds, and requires a series of data processing and modelling processes that consume computing power and time proportional to the size of the model [30]. The third method often takes time to learn from demonstration and transfer skills to the robot by using algorithms, such as dynamical movement primitives, Gaussian Mixture Model, and Hidden Markov Model [31–33], which has the disadvantage of low flexibility in real-time operation and highly personalised tasks. Based on the



FIGURE 1 An example of ultrasonic examination.

above problems, in this paper, we consider controlling the position and pose of the robot as freely as possible without relying on additional sensors. As a result, the exact position of the surface is uncertain in our following analysis.

For force control, we aim to enable a robot manipulator to accurately track the desired force under the condition that surface information, such as surface position and stiffness is uncertain. So far, various control techniques have been proposed to achieve force tracking [34], mainly falling into two categories:

- 1) Modifying the reference trajectory. For example, Jung et al. [35] proposed to adapt the reference trajectory by replacing the unknown environmental stiffness with a function of the measured force and used the local stability at equilibrium to analyse the uncertainty in environmental position. Jung et al. [36] developed a new impedance function based on the desired force to compensate for the environmental location and stiffness. Zhang et al. [37] proposed an adaptive control algorithm to generate a reference motion trajectory by minimising the force error.
- 2) Adjusting the impedance or admittance parameters. Lee et al. [38] regulated the target contact force with a variable stiffness of the impedance control based on force error. A stiffness regulation law on top of the energy-tank for impedance control was designed in ref. [39]. Li et al. [40] used gradient-following and adaptive control to obtain the desired impedance model under an unknown environment. A variable damping admittance control algorithm for the uncertain environments was proposed in ref. [41]. And in ref. [42], a novel variable impedance model was given for adaptive precision-compliance tradeoff.

When touching an uncertain environment, humans can regulate the stiffness of their arm muscles to control the contact force. Some approaches have been developed to mimic this human operation. Ajoudani et al. [43] is one of the examples that transferred the human arm stiffness information to the robot manipulator via EMG and realised human-like compliant control. Therefore, adjusting the stiffness of impedance or admittance control is more similar to human operation under an uncertain environment.

To implement the scanning tasks for uncertain surfaces, the main contributions of our work are as follows:

1. A HRC method based on teleoperation and variable stiffness compliant force tracking is developed, which can realise uncertain surface scanning without prior environmental position modelling or path planning.
2. The end-effector orientation can be adjusted automatically based on external force perception and friction force estimation.
3. A hybrid force/motion control is developed to decouple teleoperation, compliant control, and pose adjustment operations, which can reduce the workload of operators with a safety guarantee.

The remainder of this paper is organised as follows. Section 2 describes our teleoperation system. Section 3 introduces the methods of perceiving external force and estimating friction force. Section 4 presents the force tracking algorithm. In Section 5, we combine the methods and propose a hybrid force/motion controller. Section 6 verifies the method through a mock ultrasound examination experiment. Section 7 concludes this work.

2 | TELEOPERATION

Based on the principle of ease of use, we have developed an intuitive tele-operation system. Geomagic Touch X, a haptic feedback device developed by SensAble Technologies, which includes hardware drives and software packages (OpenHaptics Toolkit) [44], is used as the master device for robot teleoperation control in our work. The 6-DoF Elite robot is used as the follower. This section will establish the position and pose mapping between the Touch X joystick and the robot end-effector.

The coordinate frames of the Touch X device and the Elite robot are shown in Figure 2, in which $\{TB\}$, $\{TT\}$, $\{RB\}$, and $\{RE\}$ represent the base coordinate frame of Touch X, the coordinate frame of Touch X tip, the base coordinate frame of robot, and the end-effector frame of robot respectively. The position mapping relation is defined as:

$$\begin{aligned}\Delta\mathbf{X}_{RE} &= \frac{RE}{TB}\mathbf{R} \cdot \mathbf{S} \cdot \Delta\mathbf{X}_{TB} \\ \Delta\mathbf{X}_{RB} &= \frac{RB}{RE}\mathbf{R} \cdot \Delta\mathbf{X}_{RE}\end{aligned}\quad (1)$$

or

$$\Delta\mathbf{X}_{RB} = \frac{RB}{TB}\mathbf{R} \cdot \mathbf{S} \cdot \Delta\mathbf{X}_{TB}\quad (2)$$

where

$$\begin{aligned}\Delta\mathbf{X}_{TB} &= [\Delta X_{TB}, \Delta Y_{TB}, \Delta Z_{TB}]^T \\ \Delta\mathbf{X}_{RB} &= [\Delta X_{RB}, \Delta Y_{RB}, \Delta Z_{RB}]^T \\ \Delta\mathbf{X}_{RE} &= [\Delta X_{RE}, \Delta Y_{RE}, \Delta Z_{RE}]^T\end{aligned}\quad (3)$$

are the Cartesian displacements in the coordinate $\{TB\}$, coordinate $\{RB\}$ and coordinate $\{RE\}$, respectively; $\mathbf{S} = \text{diag}$

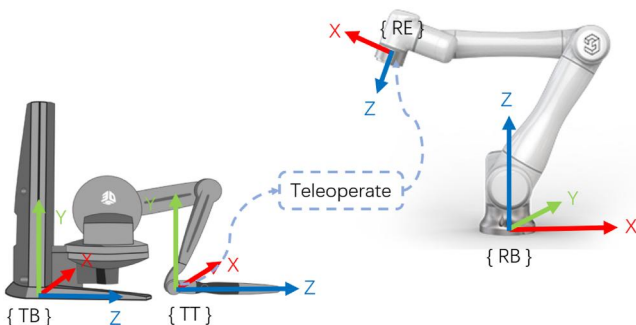


FIGURE 2 Schematic diagram of teleoperation.

(s_x, s_y, s_z) and s_x, s_y, s_z are the positive scaling factors; $\frac{RE}{TB}\mathbf{R}$ is the rotation matrix converting the translation in the workspace of Touch X to the robot end-effector workspace; $\frac{RB}{RE}\mathbf{R}$ is the rotation matrix from the robot end-effector to the robot base; and $\frac{RB}{TB}\mathbf{R}$ is the rotation matrix converting the translation in the workspace of Touch X to the robot workspace.

Representing the pose with rotation matrix, the pose mapping relation is proposed as follows:

$$\begin{aligned}\frac{TT}{RE}\mathbf{R} &= \frac{TB}{TT}\mathbf{R}_0^{-1} \cdot \frac{RB}{TB}\mathbf{R}^{-1} \cdot \frac{RB}{RE}\mathbf{R}_0 \\ \frac{RB}{RE}\mathbf{R} &= \frac{RB}{TB}\mathbf{R} \cdot \frac{TB}{TT}\mathbf{R} \cdot \frac{TT}{RE}\mathbf{R}\end{aligned}\quad (4)$$

where $\frac{TB}{TT}\mathbf{R}$ and $\frac{RB}{RE}\mathbf{R}$ represent the initial poses of Touch X tip and robot end-effector at the beginning of the teleoperation process, while $\frac{TB}{TT}\mathbf{R}_0$ and $\frac{RB}{RE}\mathbf{R}_0$ represent the real-time poses during teleoperation. $\frac{RE}{TB}\mathbf{R}$ and $\frac{RB}{TB}\mathbf{R}$ are set according to the relative placement of robot and Touch X. This mapping strategy allows the end-effector to change its pose following the joystick intuitively.

To overcome the problem of the robot and Touch X workspaces being very different, a phase operation method is used, that is when the button on the Touch X joystick is pressed, the teleoperation is performed, and when the button is released, the joystick can be moved to a suitable position freely in preparation for the next teleoperation.

In the practical application, in the following section, the robot end-effector coordinate frame $\{RE\}$ will be used as the end-of-tool coordinate for convenience.

3 | EXTERNAL FORCE PERCEPTION AND FRICTION ESTIMATION

3.1 | External force perception

The external force applied to the robot end-effector is usually measured by a six-axis F/T sensor, the readings of which are often affected by several factors, including the centre of gravity of the load, sensor bias, robot end-effector orientation etc. By collecting F/T sensor data from multiple robot orientations, the load centre of gravity and sensor bias parameters can be calculated and compensated for to accurately obtain the true external force/torque [45].

The relationship between force, torque and bias is defined as:

$$\begin{bmatrix} M_x \\ M_y \\ M_z \end{bmatrix} = \begin{bmatrix} 0 & F_z & -F_y & 1 & 0 & 0 \\ -F_z & 0 & F_x & 0 & 1 & 0 \\ F_y & -F_x & 0 & 0 & 0 & 1 \end{bmatrix} \begin{bmatrix} x \\ y \\ z \\ k_1 \\ k_2 \\ k_3 \end{bmatrix}\quad (5)$$

where

$$\begin{cases} k_1 = M_{x0} + F_{y0} \times z - F_{z0} \times y \\ k_2 = M_{y0} + F_{z0} \times x - F_{x0} \times z \\ k_3 = M_{z0} + F_{x0} \times y - F_{y0} \times x \end{cases} \quad (6)$$

(F_x, F_y, F_z) is three-dimensional forces, (M_x, M_y, M_z) is three-dimensional torques. (x, y, z) represent the centre of gravity of the load in the sensor coordinate. $F_{x0}, F_{y0}, F_{z0}, M_{x0}, M_{y0},$ and M_{z0} correspond to the bias of each force/torque component. Control the robot with load to get $N(N \geq 3)$ different poses and N corresponding sets of F/T sensor data, then we have:

$$\begin{bmatrix} M_{x1} \\ M_{y1} \\ M_{z1} \\ M_{x2} \\ M_{y2} \\ M_{z2} \\ \vdots \\ M_{xN} \\ M_{yN} \\ M_{zN} \end{bmatrix} = \begin{bmatrix} 0 & F_{z1} & -F_{y1} & 1 & 0 & 0 \\ -F_{z1} & 0 & F_{x1} & 0 & 1 & 0 \\ F_{y1} & -F_{x1} & 0 & 0 & 0 & 1 \\ 0 & F_{z2} & -F_{y2} & 1 & 0 & 0 \\ -F_{z2} & 0 & F_{x2} & 0 & 1 & 0 \\ F_{y2} & -F_{x2} & 0 & 0 & 0 & 1 \\ \vdots & \vdots & \vdots & \vdots & \vdots & \vdots \\ 0 & F_{zN} & -F_{yN} & 1 & 0 & 0 \\ -F_{zN} & 0 & F_{xN} & 0 & 1 & 0 \\ F_{yN} & -F_{xN} & 0 & 0 & 0 & 1 \end{bmatrix} \begin{bmatrix} x \\ y \\ z \\ k_1 \\ k_2 \\ k_3 \end{bmatrix} \quad (7)$$

For brevity, it can be expressed as:

$$\mathbf{m} = \mathbf{F}\mathbf{p} \quad (8)$$

where

$$\mathbf{p} = [x \ y \ z \ k_1 \ k_2 \ k_3]^T \quad (9)$$

premultiply \mathbf{F}^T on both sides of Equation (8), yields

$$\mathbf{p} = (\mathbf{F}^T \mathbf{F})^{-1} \mathbf{F}^T \mathbf{m} \quad (10)$$

Thus, the coordinates of the load centre of gravity (x, y, z) and constants k_1, k_2, k_3 are obtained.

Assuming that the robot base is placed parallel to the ground, so the relationship between sensor data, load gravity and robot end-effector orientation is defined as:

$$\begin{bmatrix} F_x \\ F_y \\ F_z \end{bmatrix} = {}^{RB}_{RE} \mathbf{R}^T \begin{bmatrix} 0 \\ 0 \\ -G \end{bmatrix} + \begin{bmatrix} F_{x0} \\ F_{y0} \\ F_{z0} \end{bmatrix} = \begin{bmatrix} {}^{RB}_{RE} \mathbf{R}^T & | & \mathbf{I} \end{bmatrix} \begin{bmatrix} 0 \\ 0 \\ -G \\ F_{x0} \\ F_{y0} \\ F_{z0} \end{bmatrix} \quad (11)$$

where G is the gravity magnitude, and \mathbf{I} is a 3-tuple identity matrix. Similarly, take N different poses and sensor data. Then, we get:

$$\begin{bmatrix} F_{x1} \\ F_{y1} \\ F_{z1} \\ F_{x2} \\ F_{y2} \\ F_{z2} \\ \vdots \\ F_{xN} \\ F_{yN} \\ F_{zN} \end{bmatrix} = \begin{bmatrix} {}^{RB}_{RE} \mathbf{R}_1^T & | & \mathbf{I} \\ {}^{RB}_{RE} \mathbf{R}_2^T & | & \mathbf{I} \\ \vdots & \vdots & \vdots \\ {}^{RB}_{RE} \mathbf{R}_N^T & | & \mathbf{I} \end{bmatrix} \begin{bmatrix} 0 \\ 0 \\ -G \\ F_{x0} \\ F_{y0} \\ F_{z0} \end{bmatrix} \quad (12)$$

it equals to

$$\mathbf{f} = \mathbf{R}\mathbf{a} \quad (13)$$

where

$$\mathbf{a} = [0 \ 0 \ -G \ F_{x0} \ F_{y0} \ F_{z0}]^T \quad (14)$$

premultiply \mathbf{R}^T on both sides of Equation (14), yields

$$\mathbf{a} = (\mathbf{R}^T \mathbf{R})^{-1} \mathbf{R}^T \mathbf{f} \quad (15)$$

Hence the gravity magnitude G and the bias of F/T sensor F_{x0}, F_{y0}, F_{z0} are obtained. Then M_{x0}, M_{y0}, M_{z0} can be calculated with Equation (6):

$$\begin{cases} M_{x0} = k_1 - F_{y0} \times z + F_{z0} \times y \\ M_{y0} = k_2 - F_{z0} \times x + F_{x0} \times z \\ M_{z0} = k_3 - F_{x0} \times y + F_{y0} \times x \end{cases} \quad (16)$$

During the robot control process, the bias and the load gravity can be compensated in real-time with the parameters calculated above. It is easy to derive that the gravity force components and torque components in the F/T sensor coordinate are:

$$\begin{bmatrix} F_{gx} \\ F_{gy} \\ F_{gz} \end{bmatrix} = {}^{RB}_{RE} \mathbf{R}^T \begin{bmatrix} 0 \\ 0 \\ -G \end{bmatrix} \quad (17)$$

$$\begin{cases} M_{gx} = F_{gz} \times y - F_{gy} \times z \\ M_{gy} = F_{gx} \times z - F_{gz} \times x \\ M_{gz} = F_{gy} \times x - F_{gx} \times y \end{cases} \quad (18)$$

Therefore, the actual external forces acting on the F/T sensor are:

$$\begin{cases} F_{cx} = F_x - F_{x0} - F_{gx} \\ F_{cy} = F_y - F_{y0} - F_{gy} \\ F_{cz} = F_z - F_{z0} - F_{gz} \end{cases} \quad (19)$$

And the actual external torques are:

$$\begin{cases} M_{ex} = M_x - M_{x0} - M_{gx} \\ M_{ey} = M_y - M_{y0} - M_{gy} \\ M_{ez} = M_z - M_{z0} - M_{gz} \end{cases} \quad (20)$$

In consequence, the external force and torque are perceived.

3.2 | Friction identification

The contact sliding friction force between the tool and the surface may affect the autonomous orientation adjustment of the tool. Due to the unknown surface properties, the friction force should first be identified so that it can be eliminated during scanning. Assuming that the surface has uniform properties and that the scanning friction satisfies the Coulomb friction model, that is the resistive force F_f due to Coulomb friction is a function of the sliding velocity v and has a constant magnitude $\mu_k F_N$, where μ_k is the kinetic friction coefficient and F_N is the normal pressure, that is

$$\begin{cases} F_f = -\mu_k F_N, & v < 0 \\ F_f = \mu_k F_N, & v > 0 \end{cases} \quad (21)$$

Owing to complex situations of the unknown surface, it is difficult to decompose the exact friction force from the external force. So an estimated value will be given instead. If the tool is always perpendicular to the surface while sliding, it can be assumed that

$$F_N = F_{ez} \quad (22)$$

$$F_f = \sqrt{F_{ex}^2 + F_{ey}^2} \quad (23)$$

so the kinetic friction coefficient $\hat{\mu}_k$ can be estimated by using b groups of F/T sensor data, which is defined as:

$$\hat{\mu}_k = \frac{1}{b} \sum_{i=1}^b \left| \frac{F_{fi}}{F_{Ni}} \right| \quad (24)$$

where i represents the sample time.

The teleoperation strategy described in the last section is applied to keep the tool perpendicular to the surface for collecting the F/T sensor data during sliding. More specifically, we adapt the orientation of the tool manually in a small area of the surface to identify the sliding friction. Considering the mechanical structural limitation of the master device Touch X, we provide the robot a constant velocity in the XY plane of coordinate $\{RE\}$, which decouples the motion of two dimensions in the Touch X workspace and enables a more convenient operation for the operator. Figure 3 shows the schematic diagram of friction identification.

In static contact, friction is negligible and therefore does not need to be compensated. To obtain external contact force

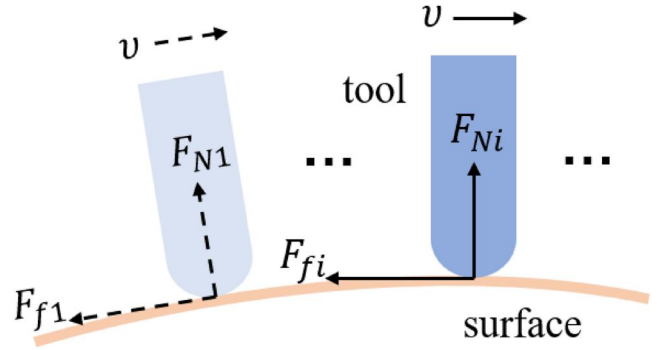


FIGURE 3 Schematic diagram of friction identification.

in the dynamic contact state, a friction force compensation law is used:

$$\begin{cases} F'_{ex} = \frac{F_{ex}}{|F_{ex}|} \left(|F_{ex}| - \left| \hat{\mu}_k \cos \left(\arctan \frac{v_y}{v_x} \right) F_{ez} \right| \right), & v_x > 0 \\ F'_{ey} = \frac{F_{ey}}{|F_{ey}|} \left(|F_{ey}| - \left| \hat{\mu}_k \sin \left(\arctan \frac{v_y}{v_x} \right) F_{ez} \right| \right), & v_y > 0 \end{cases} \quad (25)$$

which means the friction force is compensated in each motion direction. To simplify the expression, $\mathbf{F}_e = [F_{ex}, F_{ey}, F_{ez}]^T$ will be used to represent the external contact force after filtering and the compensation of sensor bias, load gravity and friction force.

4 | FORCE CONTROL

In most applications, contact force control is a key part of surface scanning. The robotic dynamics model, environment model, and an adaptive admittance control model for the uncertain environments will be discussed in this section to realise the tracking of the desired force profile with the surface.

The general dynamics model of an 6-DoF robotic manipulator in Cartesian space is given by

$$\mathbf{H}(\mathbf{x})\ddot{\mathbf{x}} + \mathbf{C}(\mathbf{x}, \dot{\mathbf{x}})\dot{\mathbf{x}} + \mathbf{g}(\mathbf{x}) = \mathbf{F}_\tau + \mathbf{F}_e \quad (26)$$

where $\mathbf{x} \in R^6$ is the Cartesian vector of the end-effector. $\mathbf{H}(\mathbf{x})$ is the Cartesian inertia matrix; $\mathbf{C}(\mathbf{x}, \dot{\mathbf{x}})$ is the Cartesian Coriolis and centrifugal matrix; $\mathbf{g}(\mathbf{x})$ is the Cartesian gravity vector; and \mathbf{F}_τ represents the Cartesian driving force.

The admittance relationship between the position and force of the close-loop robot system in Cartesian space is modelled as

$$\mathbf{M}\ddot{\mathbf{e}} + \mathbf{B}\dot{\mathbf{e}} + \mathbf{K}\mathbf{e} = \mathbf{F}_e \quad (27)$$

where \mathbf{M} , \mathbf{B} , and \mathbf{K} are the mass, damping and stiffness matrices respectively. And $\mathbf{e} = \mathbf{x}_c - \mathbf{x}_r$ represents the error between the actual commanded position and the desired

reference position, in which we assume that the robot can accurately track the commanded position trajectory in position control mode, namely $\mathbf{x} \approx \mathbf{x}_c$.

For simplicity, we consider 1-DoF as below,

$$m\ddot{e} + b\dot{e} + ke = f_e \quad (28)$$

When the admittance control system reaches the steady state, namely $\ddot{x}_c = 0$ and $\dot{x}_c = 0$, so Equation (28) becomes

$$k(x_c - x_r) = f_e \quad (29)$$

Generally, the environment in one direction can be modelled as a one-dimensional linear spring model with stiffness k_e , which is defined as

$$f_e = k_e(x_e - x) \quad (30)$$

where x_e is the environment position.

The contact force can be regulated by adjusting the robot end-effector position which is controlled by the admittance controller via force feedback. So combining Equations (29) and (30), we can obtain the steady-state external contact force as

$$f_e = \frac{k k_e (x_e - x_r)}{k + k_e} \quad (31)$$

Observing Equation (31), both k_e and x_e are environmental parameters, which are uncontrollable. Thus, we can consider two strategies to regulate the f_e : (1) modifying the reference position trajectory x_r ; (2) adjusting the admittance stiffness k .

For the first method, the unknown environmental location adds difficulty to the design of reference trajectory. Therefore, an admittance-based controller with variable stiffness is adopted in our work which has the form of

$$b\dot{e} + k_v e = f_e \quad (32)$$

where the mass term is omitted and k_v represents the on-line variable stiffness.

The force error is defined as

$$\Delta f = f_e - f_d \quad (33)$$

Substituting Equation (32) into Equation (33), the closed-loop control system can be obtained as:

$$\Delta f = b\dot{e} + k_v e - f_d \quad (34)$$

where the control law of k_v is defined as

$$k_v = -\frac{k_p \Delta f + k_i \int_0^t \Delta f dt + k_d \Delta \dot{f}}{e} \quad (35)$$

where k_p , k_i , and k_d are constant proportional, integral and differential gains. Substituting Equation (35) into Equation (34), the close-loop control system becomes

$$(k_p + 1)\Delta f + k_i \int_0^t \Delta f dt + k_d \Delta \dot{f} = b\dot{e} - f_d \quad (36)$$

The reference trajectory x_r is designed as a fix position, so the corresponding acceleration and velocity are $\ddot{x}_r = 0$ and $\dot{x}_r = 0$. Therefore, the commanded trajectory at the time t can be generated by the admittance control law:

$$\begin{cases} \dot{x}_c(t) = \frac{(k_p + 1)\Delta f(t) + k_i \int_0^t \Delta f(t) dt + k_d \Delta \dot{f}(t) + f_d(t)}{b} \\ x_c(t) = x_c(t-1) + \dot{x}_c(t)\Delta t \end{cases} \quad (37)$$

where Δt is the system sampling period.

Please see ref. [46] for the detail.

5 | HYBRID FORCE/MOTION CONTROL

In the previous sections, we have discussed position and pose transformation of the robot by teleoperation, and the relationship between force and position in admittance control. These operations cannot be performed simultaneously on the robot, which would otherwise lead to position coupling. Therefore, in this section, a hybrid force/motion control method is proposed to decouple force control from teleoperation, while at the same time enabling the robot to achieve autonomous pose adjustment according to external forces, thus reducing workload and improving efficiency. The overall diagram of the proposed method is shown in Figure 4.

For position control, we apply teleoperation along the X and Y directions of end-effector coordinate $\{RE\}$ and the force control is utilised along the Z direction of coordinate $\{RE\}$. Specifically, by combining Equation (1) and, the position control can be expressed as

$$\Delta \mathbf{X}_{RE} = \frac{RE}{TB} \mathbf{R} \mathbf{S} \Delta \mathbf{X}_{TB} \lambda' + \dot{\mathbf{x}}_c \Delta t \lambda \quad (38)$$

where

$$\lambda' = \begin{bmatrix} 1 & & \\ & 1 & \\ & & 0 \end{bmatrix}, \quad \lambda = \begin{bmatrix} 0 & & \\ & 0 & \\ & & 1 \end{bmatrix} \quad (39)$$

Due to the possibility of collision during movement, classical admittance control is added to the X and Y directions for the safety of the robot and the object. ΔX_{RE} and ΔY_{RE} are regarded as the desired position x_r of the admittance control in corresponding directions. So Equation (38) becomes

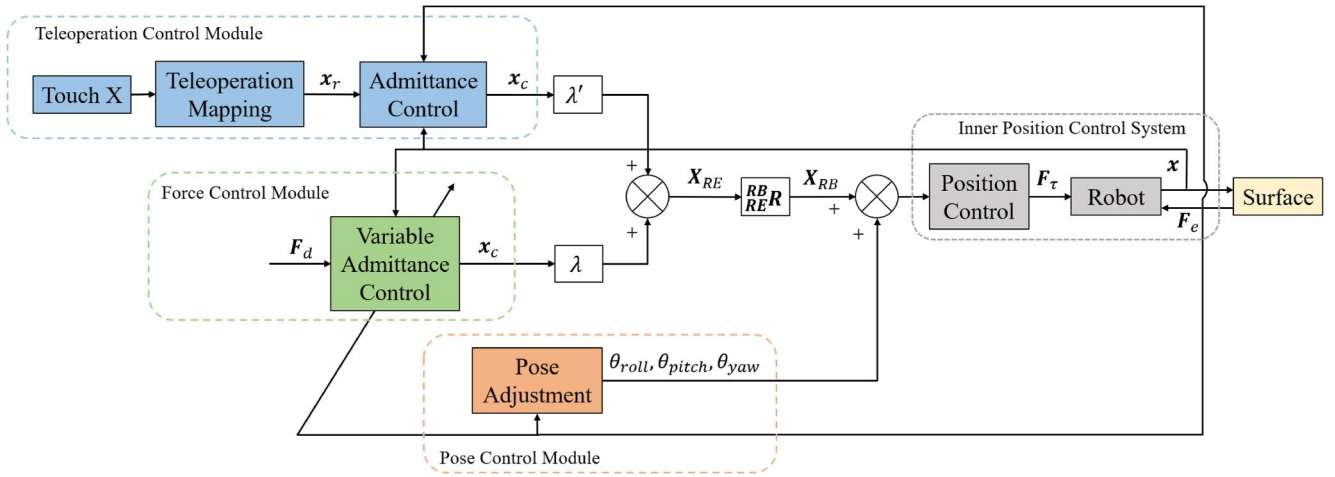


FIGURE 4 Diagram of the proposed method.

$$\Delta \mathbf{X}_{RE} = \left({}^{RE}_{TB} \mathbf{R} \mathbf{S} \Delta \mathbf{X}_{TB} + \mathbf{e} \right) \lambda' + \dot{\mathbf{x}}_c \Delta t \lambda \quad (40)$$

It can be represented in the robot base coordinate $\{RB\}$ using Equation (2), thus the target position \mathbf{X}_{tar} is given by

$$\mathbf{X}_{tar} = \mathbf{X}_{cur} + {}^{RB}_{RE} \mathbf{R} \Delta \mathbf{X}_{RE} \quad (41)$$

where \mathbf{X}_{cur} is the current manipulator position.

Consequently, the robot can track the position through inverse kinematic and inner position controller.

For pose control, the direction of tool is designed to rotate following the direction of the resultant external force. Figure 5 shows the rotation process. The current direction \mathbf{V}_{cur} the target direction \mathbf{V}_{tar} under coordinate $\{RE\}$ are formulated as follows:

$$\mathbf{V}_{cur} = [0, 0, 1]^T \quad (42)$$

$$\mathbf{V}_{tar} = [-F_{ex}, -F_{ey}, -F_{ez}]^T \quad (43)$$

The rotation axis that the tool rotates around is defined as follows:

$$\mathbf{V}_{rot} = [V_x, V_y, V_z]^T = \mathbf{V}_{cur} \times \mathbf{V}_{tar} \quad (44)$$

The rotation angle value is defined as

$$\theta = \min \left(\arccos \frac{\mathbf{V}_{cur} \mathbf{V}_{tar}}{\|\mathbf{V}_{cur}\| \|\mathbf{V}_{tar}\|}, \theta_{thresh} \right) \quad (45)$$

where θ_{thresh} is an angle threshold to avoid the sudden pose changes of tool which may cause danger.

With the rotation axis and the rotation angle, the rotation matrix from \mathbf{V}_{cur} to \mathbf{V}_{tar} can be calculated through the Rodrigues' rotation formula, which is

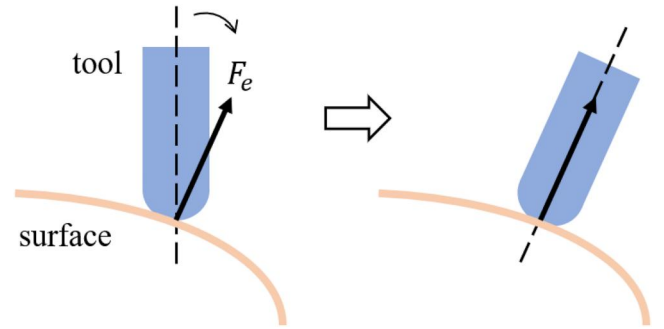


FIGURE 5 Schematic diagram of pose adjustment of the tool.

$$\begin{aligned} {}^{RE}_{RE'} \mathbf{R} &= \begin{bmatrix} r_{11} & r_{12} & r_{13} \\ r_{21} & r_{22} & r_{23} \\ r_{31} & r_{32} & r_{33} \end{bmatrix} \\ &= \mathbf{I} + \sin \theta \mathbf{M}_v + (1 - \cos \theta) \mathbf{M}_v^2 \end{aligned} \quad (46)$$

where

$$\mathbf{M}_v = \begin{bmatrix} 0 & -V_z & V_y \\ V_z & 0 & -V_x \\ -V_y & V_x & 0 \end{bmatrix} \quad (47)$$

Transform it to the robot base coordinate by

$${}^{RB}_{RE'} \mathbf{R} = {}^{RB}_{RE} \mathbf{R} \cdot {}^{RE}_{RE'} \mathbf{R} \quad (48)$$

then it can be converted into Euler angles and sent to the robot position controller:

$$\begin{aligned} \theta_{pitch} &= \text{atan2} \left(-r_{31}, \sqrt{r_{11}^2 + r_{21}^2} \right) \\ \theta_{roll} &= \text{atan2} \left(r_{32} / \cos(\theta_{pitch}), r_{33} / \cos(\theta_{pitch}) \right) \\ \theta_{yaw} &= \text{atan2} \left(r_{32} / \cos(\theta_{pitch}), r_{33} / \cos(\theta_{pitch}) \right) \end{aligned} \quad (49)$$

Through these arrangements, the force control, teleoperation and pose adjustment of the robot are independent which can be carried out in a reasonable manner without position coupling.

6 | EXPERIMENTS

The proposed method was validated through a mock B-ultrasound scanning experiment on a phantom. Traditional B-ultrasound scanning examination requires the sonographers to hold a transducer probe for skin surface scanning of patients with proper contact force, and pay attention to the images in the ultrasound imaging equipment in the meantime, which is physically challenging for them to keep the arm muscles tight and maintain an uncomfortable scanning posture. Consequently, the long-term operation may result in muscle fatigue or injury [7]. Additionally, close contact with patients may not ensure the safety of the sonographers in some cases such as epidemics period.

The experimental setup is shown in Figure 6, which consists of a console, a 6-DoF Elite® robot, a master device Touch X, an ATI® mini45 F/T sensor, a probe, and a phantom with uncertain properties. The coordinate frames of the robot base, end-effector, F/T sensor, and Touch X are $\{RB\}$, $\{RE\}$, $\{SS\}$, and $\{TB\}$ respectively. In particular, $\{RE\}$ is aligned with $\{SS\}$. Both the Touch X and the robot communicate with the controller through EtherCAT. The F/T sensor and the controller communicate through TCP/IP protocol with sample rate of 1000 Hz. The robot control cycle is 20 ms.

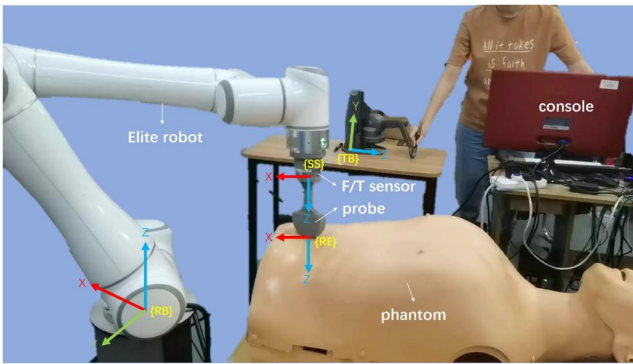


FIGURE 6 Experiment setup.

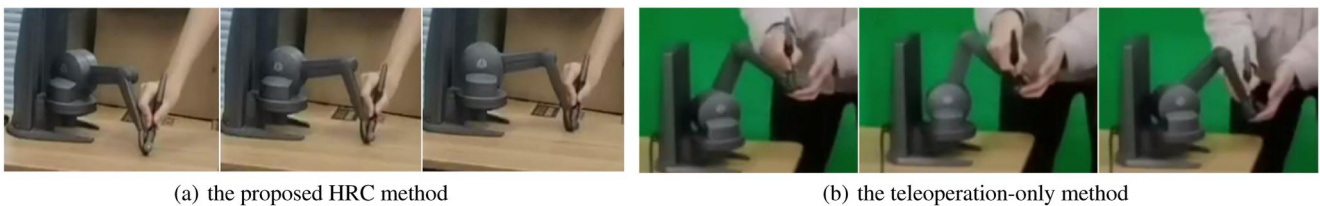


FIGURE 7 Operation process.

In the experiment, we identified the kinetic friction coefficient μ_k of phantom first, and the value was 0.6. The desired contact force in z axis was set $f_d = -5\text{N}$. The scaling factor S_x and S_y were set 4. The parameters of the force-tracking controller were set $k_p = 0.08$, $k_i = 0.1$, $k_d = 0.3$, $b = 100$. ${}^{RE}_{TB}\mathbf{R}$ and ${}^{RB}_{TB}\mathbf{R}$ were given by

$${}^{RE}_{TB}\mathbf{R} = \begin{bmatrix} 0 & 0 & -1 \\ 1 & 0 & 0 \\ 0 & -1 & 0 \end{bmatrix}, \quad {}^{RB}_{TB}\mathbf{R} = \begin{bmatrix} 0 & 0 & -1 \\ -1 & 0 & 0 \\ 0 & 1 & 0 \end{bmatrix} \quad (50)$$

During the task, the operator holds the Touch X joystick and move it in the XZ plane of coordinate $\{TB\}$. As shown in Figure 7a, the operator can slide the gimbal of joystick on the desk with muscle relaxation. The movement along the Z axis of coordinate $\{RE\}$ and the direction adjustment will be automatically conducted by the robot.

The effectiveness of the proposed method was verified by controlling the manipulator to scan back and forth on the skin surface of the belly and the chest of the phantom, and the experiment performances are shown in Figures 8 and 9. The belly and the chest surface were irregular and they are supported by sponges and springs respectively. However, the probe remained approximately perpendicular to the surface and moved steadily all the time without trajectory planning and visual model in advance.

The corresponding results are shown in Figure 10a,b. Once the probe contacted with the surface, an initial overshoot happened, but the force settled to about -5N in approximately 3 s. The maximum force on the belly and the chest reached about 10N and 13N, which were within the safe limits of human body. The force error of steady state was within $\pm 1\text{N}$ most of time, occasionally within $\pm 2\text{N}$ due to the complex environment and dynamic process.

To further verify the validity of our proposed HRC method, the teleoperation-only method with Equations (2) and (4) was used as a comparison. Specifically, the operator was required to control the position and pose of the robot end-effector manually through teleoperation. Figure 7b shows the operation process, in which the operator should hold the joystick of Touch X in the air and adjust it as precisely as possible. We invited four volunteers to implement the surface scanning task using the proposed HRC method and the teleoperation-only method respectively. For simplicity, they only need to scan the phantom belly along a similar trajectory. One of the experiment performances with the teleoperation-only method is shown in Figure 11. It can be seen that the

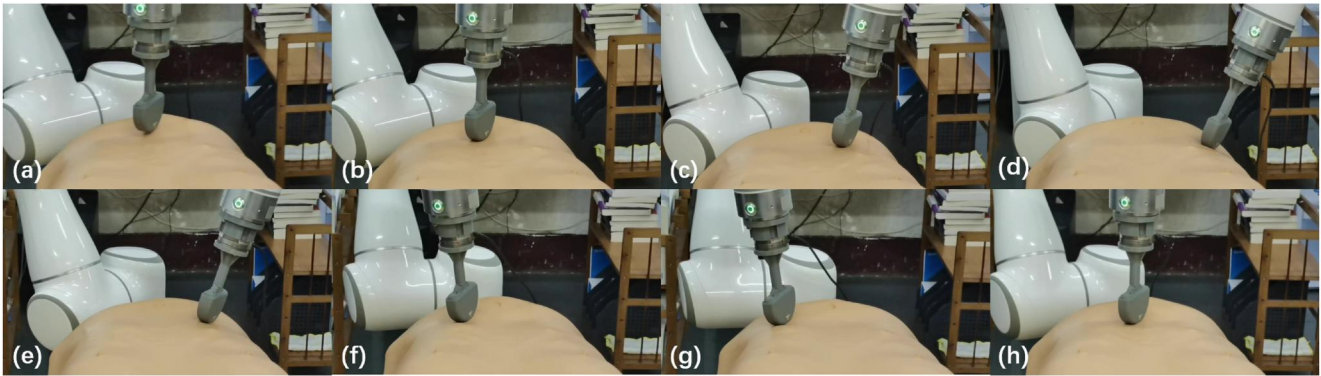


FIGURE 8 Surface scanning on belly with the proposed human-robot collaboration method.

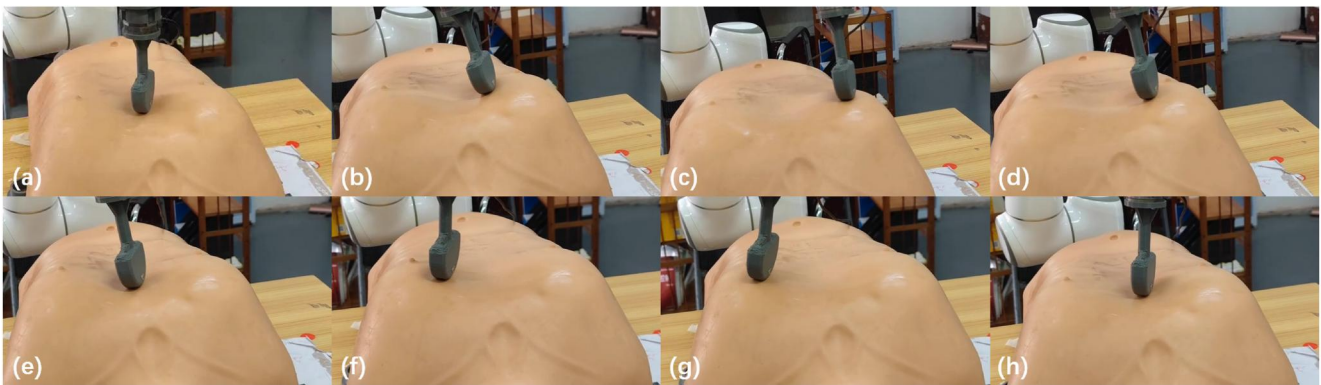


FIGURE 9 Surface scanning on chest with the proposed human-robot collaboration method.

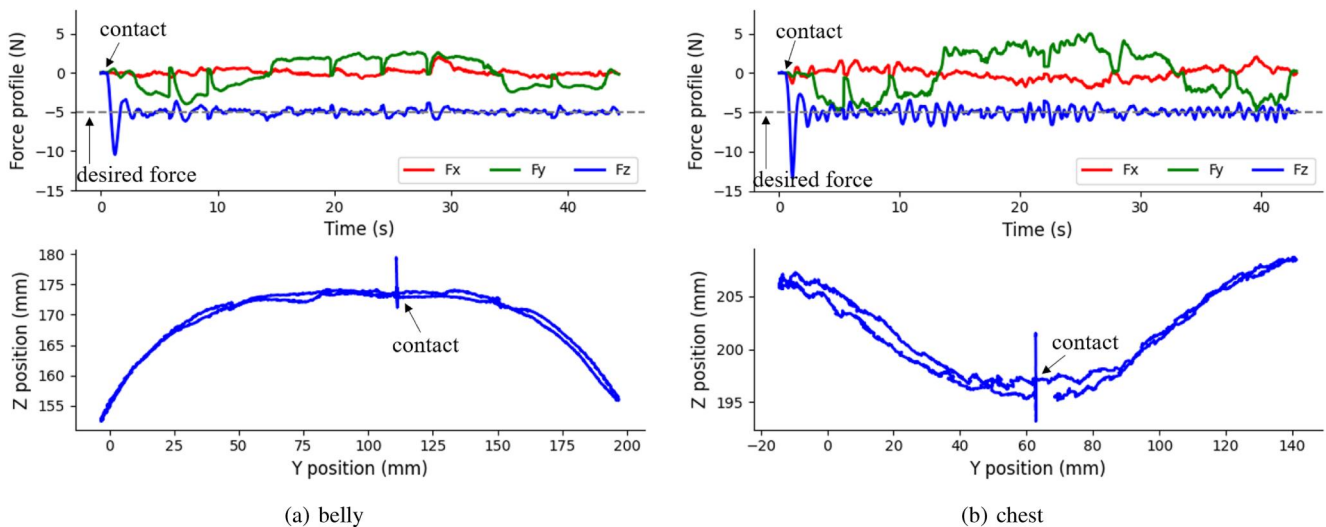


FIGURE 10 Results of surface scanning with the proposed human-robot collaboration method.

probe was moved away from or squeezed the surface sometimes instead of sliding steadily against the surface. The detailed results of the four surface scanning experiments are shown in Figure 12, where the force curves of the teleoperation-only method change over a wide range and the

position curves are rougher than our method obviously, which indicates that pure position control is unable to guarantee stable contact force and movement, thus may cause damage to the object. In contrast, our method is much safer, more reliable, and more convenient.

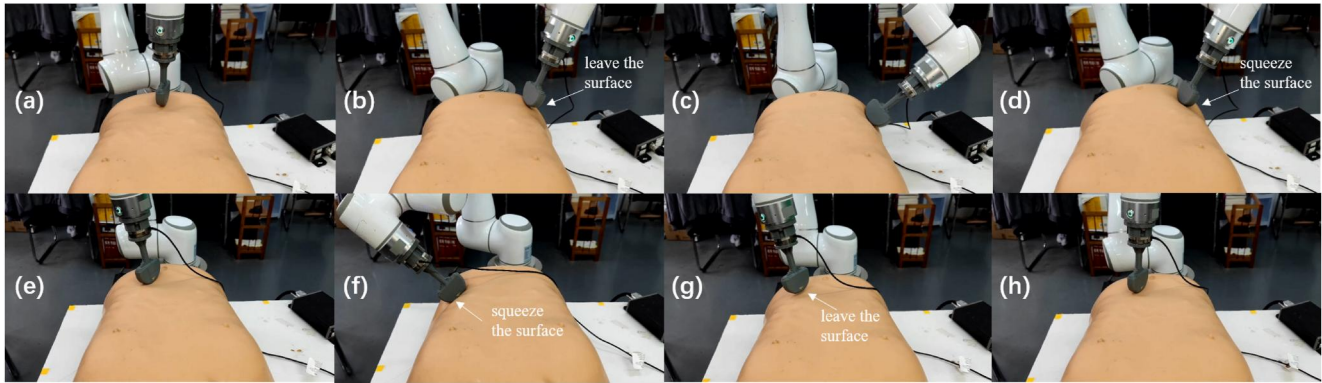


FIGURE 11 Surface scanning with the teleoperation-only method.

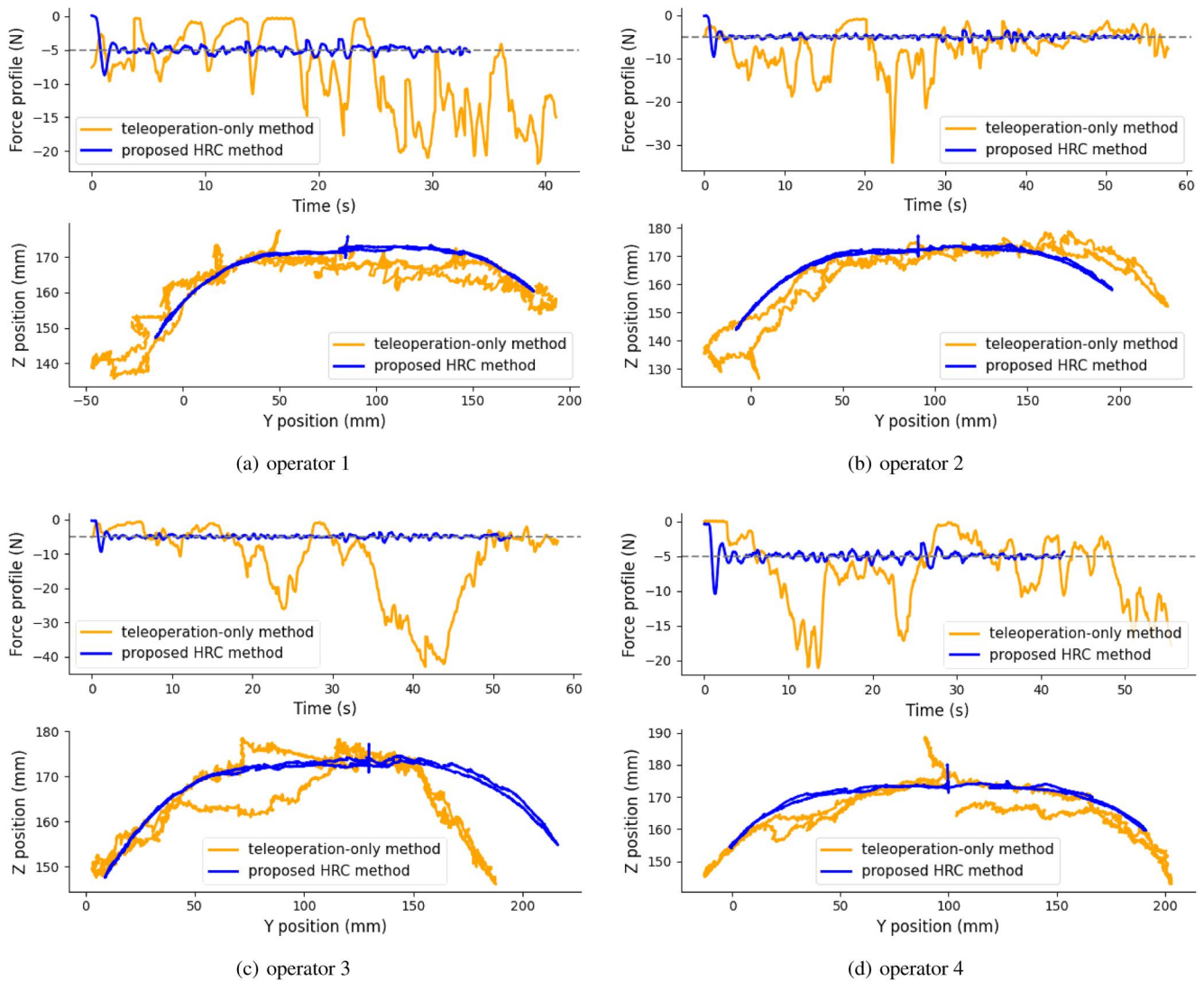


FIGURE 12 Four experiment results with two methods.

7 | CONCLUSION AND FUTURE WORK

In this paper, we propose a HRC method for uncertain surface scanning. This method transmits human intention and experience to the manipulator remotely through teleoperation, which

can separate the operators from the working environment and ensure their safety of the operators. An adaptive variable admittance control for uncertain environments is used to apply a constant force to the surface. Meanwhile, the manipulator can adjust the orientation automatically to remain approximately

perpendicular to the surface according to the external forces which are perceived through gravity and friction compensation. The hybrid force/motion control combines the technologies together, thus enabling the simultaneous control of robot position, direction, and force while reducing the operators' workload. The mock B-ultrasound scanning experiment verifies the feasibility of the method, which means the method may be applied to scanning tasks such as B-ultrasound inspection.

Our work assumes that the surface is ideally uniform with the same properties. However, the nature of the surface may vary from one situation to another in many practical situations. For instance, different parts of the human body may require varying contact forces to obtain high-quality ultrasound images, and the complex friction on the surface of a rusted workpiece may be difficult to identify. Sometimes the tool direction also needs to be fine-tuned based on the actual condition. Facing the above problems, we will develop more efficient algorithms in future work. For example, learning force control and direction adjustment strategies through multi-modal fusion deep learning methods, and identify the friction by using more dimensional sensor information.

ACKNOWLEDGMENTS

This work was partially supported by Engineering and Physical Sciences Research Council (EPSRC) under Grant EP/S001913.

CONFLICT OF INTEREST STATEMENT

The authors declare no conflicts of interest.


DATA AVAILABILITY STATEMENT

The data used to support the findings of this study are included within the article.

ORCID

Guanyi Zhao  <https://orcid.org/0000-0002-7359-8061>

Chao Zeng  <https://orcid.org/0000-0003-3648-4644>

Chenguang Yang  <https://orcid.org/0000-0001-5255-5559>

REFERENCES

- Bauer, A., Wollherr, D., Buss, M.: Human-robot collaboration: a survey. *Int. J. Humanoid Rob.* 5(01), 47–66 (2008). <https://doi.org/10.1142/s0219843608001303>
- Yang, C., et al.: Interface design of a physical human-robot interaction system for human impedance adaptive skill transfer. *IEEE Trans. Autom. Sci. Eng.* 15(1), 329–340 (2017). <https://doi.org/10.1109/tase.2017.2743000>
- Peternel, L., Petrič, T., Babič, J.: Human-in-the-loop approach for teaching robot assembly tasks using impedance control interface. In: 2015 IEEE International Conference on Robotics and Automation (ICRA), pp. 1497–1502. IEEE (2015)
- Li, Y., et al.: Building companionship through human-robot collaboration. In: *International Conference on Social Robotics*, pp. 1–7. Springer (2013)
- Qiao, H., et al.: Improving performance of robots using human-inspired approaches: a survey. *Sci. China Inf. Sci.* 65(12), 31 (2022). <https://doi.org/10.1007/s11432-022-3606-1>
- Qiao, H., et al.: Brain-inspired intelligent robotics: Theoretical analysis and systematic application. *Machine Intelligence Research* 20(1), 1–18 (2023). <https://doi.org/10.1007/s11633-022-1390-8>
- Conti, F., Park, J., Khatib, O.: Interface design and control strategies for a robot assisted ultrasonic examination system. In: *Experimental Robotics*, pp. 97–113. Springer (2014)
- Huang, J., Wang, Y., Fukuda, T.: Set-membership-based fault detection and isolation for robotic assembly of electrical connectors. *IEEE Trans. Autom. Sci. Eng.* 15(1), 160–171 (2016). <https://doi.org/10.1109/tase.2016.2602319>
- Liu, Y., Nejat, G.: Robotic urban search and rescue: a survey from the control perspective. *J. Intell. Rob. Syst.* 72(2), 147–165 (2013). <https://doi.org/10.1007/s10846-013-9822-x>
- Kong, K., Bae, J., Tomizuka, M.: A compact rotary series elastic actuator for human assistive systems. *IEEE/ASME Trans. Mechatron.* 17(2), 288–297 (2011). <https://doi.org/10.1109/tmech.2010.2100046>
- Sheridan, T.B.: *Telerobotics, Automation, and Human Supervisory Control*. MIT press (1992)
- Jiang, Z., et al.: Cutting depth monitoring based on milling force for robot-assisted laminectomy. *IEEE Trans. Autom. Sci. Eng.* 17(1), 2–14 (2020). <https://doi.org/10.1109/tase.2019.2920133>
- Guo, J., et al.: Real-time measurement and estimation of the 3d geometry and motion parameters for spatially unknown moving targets. *Aero. Sci. Technol.* 97, 105619 (2020). <https://doi.org/10.1016/j.ast.2019.105619>
- Ajoudani, A., et al.: Progress and prospects of the human-robot collaboration. *Aut. Robots* 42(5), 957–975 (2018). <https://doi.org/10.1007/s10514-017-9677-2>
- Liu, Z., et al.: Approximation-free robust synchronization control for dual-linear-motors-driven systems with uncertainties and disturbances. *IEEE Trans. Ind. Electron.* 69(10), 10500–10509 (2022). <https://doi.org/10.1109/tie.2021.3137619>
- Shi, P., et al.: Master-slave synchronous control of dual-drive gantry stage with cogging force compensation. *IEEE Trans. Syst. Man Cybern. Syst.* 53(1), 216–225 (2023). <https://doi.org/10.1109/tsmc.2022.3176952>
- Tamei, T., Shibata, T.: Fast reinforcement learning for three-dimensional kinetic human-robot cooperation with an emg-to-activation model. *Adv. Robot.* 25(5), 563–580 (2011). <https://doi.org/10.1163/016918611x558252>
- Peternel, L., Tsagarakis, N., Ajoudani, A.: Towards multi-modal intention interfaces for human-robot co-manipulation. In: 2016 IEEE/RISJ International Conference on Intelligent Robots and Systems (IROS), pp. 2663–2669. IEEE (2016)
- Zeng, C., Yang, C., Chen, Z.: Bio-inspired robotic impedance adaptation for human-robot collaborative tasks. *Sci. China Inf. Sci.* 63(7), 1–10 (2020). <https://doi.org/10.1007/s11432-019-2748-x>
- Lin, Z., Luo, J., Yang, C.: A teleoperated shared control approach with haptic feedback for mobile assistive robot. In: 2019 25th International Conference on Automation and Computing (ICAC), pp. 1–6. IEEE (2019)
- Li, W., et al.: Teleoperation system for omnidirectional mobile robot based on shared control scheme. In: 2018 IEEE 8th Annual International Conference on CYBER Technology in Automation, Control, and Intelligent Systems (CYBER), pp. 741–746. IEEE (2018)
- Rozo, L., et al.: Learning optimal controllers in human-robot cooperative transportation tasks with position and force constraints. In: 2015 IEEE/RISJ International Conference on Intelligent Robots and Systems (IROS), pp. 1024–1030. IEEE (2015)
- Duchaine, V., Gosselin, C.: Safe, stable and intuitive control for physical human-robot interaction. In: 2009 IEEE International Conference on Robotics and Automation, pp. 3383–3388. IEEE (2009)
- Si, W., Wang, N., Yang, C.: A review on manipulation skill acquisition through teleoperation-based learning from demonstration. *Cognit. Comput. Syst.* 3(1), 1–16 (2021). <https://doi.org/10.1049/ccs2.12005>
- Yang, C., et al.: Teleoperation control based on combination of wave variable and neural networks. *IEEE Trans. Syst. Man Cybern. Syst.* 47(8), 2125–2136 (2016). <https://doi.org/10.1109/tsmc.2016.2615061>
- Zeng, C., et al.: Multifingered robot hand compliant manipulation based on vision-based demonstration and adaptive force control. *IEEE Trans. Neural Networks Learn. Syst.*, 1–12 (2022). <https://doi.org/10.1109/tnls.2022.3184258>

27. Walker, M.E., Hedayati, H., Szafir, D.: Robot teleoperation with augmented reality virtual surrogates. In: 2019 14th ACM/IEEE International Conference on Human-Robot Interaction (HRI), pp. 202–210. IEEE (2019)
28. Liu, Y., Habibnezhad, M., Jebelli, H.: Brain-computer interface for hands-free teleoperation of construction robots. *Autom. Construct.* 123, 103523 (2021). <https://doi.org/10.1016/j.autcon.2020.103523>
29. González, C., et al.: Advanced teleoperation and control system for industrial robots based on augmented virtuality and haptic feedback. *J. Manuf. Syst.* 59, 283–298 (2021). <https://doi.org/10.1016/j.jmsy.2021.02.013>
30. Xiao, D., et al.: Estimating reference bony shape models for orthognathic surgical planning using 3d point-cloud deep learning. *IEEE J. Biomed. Health Inf.* 25(8), 2958–2966 (2021). <https://doi.org/10.1109/jbhi.2021.3054494>
31. Ijspeert, A.J., Nakanishi, J., Schaal, S.: Movement imitation with nonlinear dynamical systems in humanoid robots. In: Proceedings 2002 IEEE International Conference on Robotics and Automation (Cat. No. 02CH37292), vol. 2, pp. 1398–1403. IEEE (2002)
32. Kyrarini, M., et al.: Robot learning of industrial assembly task via human demonstrations. *Aut. Robots* 43(1), 239–257 (2019). <https://doi.org/10.1007/s10514-018-9725-6>
33. Rozo, L., Jiménez, P., Torras, C.: A robot learning from demonstration framework to perform force-based manipulation tasks. *Intell. Serv. Robot.* 6(1), 33–51 (2013). <https://doi.org/10.1007/s11370-012-0128-9>
34. Li, M., et al.: A stability and safety control method in robot-assisted decompressive laminectomy considering respiration and deformation of spine. *IEEE Trans. Autom. Sci. Eng.* 20(1), 258–270 (2023). <https://doi.org/10.1109/tase.2022.3147270>
35. Jung, S., Hsia, T.C., Bonitz, R.G.: Force tracking impedance control for robot manipulators with an unknown environment: theory, simulation, and experiment. *Int. J. Robot Res.* 20(9), 765–774 (2001). <https://doi.org/10.1177/02783640122067651>
36. Jung, S., Hsia, T.C., Bonitz, R.G.: Force tracking impedance control of robot manipulators under unknown environment. *IEEE Trans. Control Syst. Technol.* 12(3), 474–483 (2004). <https://doi.org/10.1109/tcst.2004.824320>
37. Zhang, X., Khamesee, M.B.: Adaptive force tracking control of a magnetically navigated microrobot in uncertain environment. *IEEE ASME Trans. Mechatron.* 22(4), 1644–1651 (2017). <https://doi.org/10.1109/tmech.2017.2705523>
38. Lee, K., Buss, M.: Force tracking impedance control with variable target stiffness. *IFAC Proc. Vol.* 41(2), 6751–6756 (2008). <https://doi.org/10.3182/20080706-5-kr-1001.01144>
39. Ferraguti, F., Secchi, C., Fantuzzi, C.: A tank-based approach to impedance control with variable stiffness. In: 2013 IEEE International Conference on Robotics and Automation, pp. 4948–4953. IEEE (2013)
40. Li, Y., Ge, S.S.: Impedance learning for robots interacting with unknown environments. *IEEE Trans. Control Syst. Technol.* 22(4), 1422–1432 (2013). <https://doi.org/10.1109/tcst.2013.2286194>
41. Duan, J., et al.: Adaptive variable impedance control for dynamic contact force tracking in uncertain environment. *Robot. Autonom. Syst.* 102, 54–65 (2018). <https://doi.org/10.1016/j.robot.2018.01.009>
42. Jin, Z., et al.: Model predictive variable impedance control of manipulators for adaptive precision-compliance tradeoff. *IEEE ASME Trans. Mechatron.*, 1–13 (2022)
43. Ajoudani, A., Tzagarakis, N., Bicchi, A.: Tele-impedance: teleoperation with impedance regulation using a body-machine interface. *Int. J. Robot. Res.* 31(13), 1642–1656 (2012). <https://doi.org/10.1177/0278364912464668>
44. Hirche, S., Buss, M.: Human-oriented control for haptic teleoperation. *Proc. IEEE* 100(3), 623–647 (2012). <https://doi.org/10.1109/jproc.2011.2175150>
45. Lijian, Z., et al.: Research on force sensing for the end-load of industrial robot based on a 6-axis force/torque sensor. *Acta Autom. Sin.* 43(3), 439–447 (2017)
46. Zhang, X., et al.: Admittance-based pid variable stiffness control for force-tracking interaction with unknown environments. In: 15th International Workshop on Human-Friendly Robotics (2022)

How to cite this article: Zhao, G., et al.: A human-robot collaboration method for uncertain surface scanning. *CAAI Trans. Intell. Technol.* 1–12 (2023). <https://doi.org/10.1049/cit2.12227>